ATLAS NOTE

ATLAS-CONF-2012-085

1 July 2012

Search for dark matter candidates and large extra dimensions in events with a photon and missing transverse momentum in pp collision data at $\sqrt{s}$ =7 TeV with the ATLAS detector

The ATLAS Collaboration

Abstract

We report results of the search for new phenomena in events with an energetic photon and large missing transverse momentum in proton-proton collisions at $\sqrt{s}$ = 7 TeV. Data from the ATLAS experiment corresponding to an integrated luminosity of 4.6 fb^{-1} are used. Good agreement is observed between the data and the Standard Model predictions for the background. The results are translated into exclusion limits on models with large extra spatial dimensions and the pair production of weakly interacting dark matter candidates.

This note was modified on 31st July because of an error in the formula for the WIMP pair-production cross section, as implemented in the MADGRAPH event generator, affecting the results for the D9 operator.

ATLAS-CONF-2012-085
01/08/2012

1 Introduction

Events with an energetic photon and large missing momentum in the final state constitute a clean and distinctive signature in searches for new physics at colliders. In particular, monophoton and monojet final states have been studied [1, 2, 3, 4, 5, 6, 7, 8] in the context of searches for supersymmetry, large extra spatial dimensions (LED), and dark matter (DM), to address some of the most fundamental questions in elementary particle physics and cosmology.

The Arkani-Hamed, Dimopoulos, and Dvali model (ADD) for LED [9] provides a possible solution to the mass hierarchy problem. It explains the large difference between the electroweak unification scale $O(10^2)$ GeV and the Planck scale, $M_{Pl} \sim O(10^{19})$ GeV, by postulating the presence of n extra spatial dimensions of size R, and defining a fundamental Planck scale in $4+n$ dimensions, M_D, given by ${M_{Pl}}^2 \sim {M_D}^{2+n}R^n$. An appropriate choice of R for a given n allows for a value of M_D at the electroweak scale. The extra spatial dimensions are compactified, resulting in a Kaluza-Klein tower of massive graviton modes. At hadron colliders, these graviton modes escape detection and can be produced in association with an energetic photon or a jet, leading to a monophoton or monojet signature in the final state.

The presence of a non-baryonic DM component in the Universe is inferred from the observation of its gravitational interactions [10], but its nature is otherwise unknown. A weakly interacting massive particle (WIMP) χ with mass m_χ in the range between 1 GeV and few TeV could be a plausible candidate for DM. It could be detected via its scattering with heavy nuclei [11], the detection of cosmic rays (energetic photons, electrons, positrons, protons, antiprotons, or neutrinos) from $\chi\bar{\chi}$ annihilation in astrophysical sources, or via its pair-production at colliders. For the latter, the WIMPs do not interact with the detector and the event is identified via the presence of an energetic photon or jet from initial-state radiation. The interaction of WIMPs with standard model (SM) particles is assumed to be driven by a very massive mediator and described using a non-renormalizable effective theory [12] with several operators. The vertex coupling is suppressed by an effective cut-off mass scale $M_* \sim M/\sqrt{g_1 g_2}$, where M denotes the mass of the mediator and g_1 and g_2 are the couplings of the mediator to the WIMP and SM particles, respectively.

This note reports results on the search for new phenomena in monophoton final states, based on $\sqrt{s} = 7$ TeV proton-proton collision data corresponding to an integrated luminosity of 4.6 fb^{-1} collected with the ATLAS detector at the LHC during 2011.

2 Experimental setup

The ATLAS detector is described in detail elsewhere [13]. It consists of an inner tracking detector surrounded by a superconducting solenoid providing a 2 T magnetic field, electromagnetic and hadron calorimeters, and a muon spectrometer immersed in a toroidal magnetic field.

3 Object reconstruction and event selection

The data are collected using a three-level trigger system that selects events with uncorrected missing transverse momentum $E_T^{\text{miss}} > 70$ GeV. Offline the events are required to have $E_T^{\text{miss}} > 150$ GeV (for which the trigger selection is more than 98% efficient, as determined using events selected with a muon trigger) and a photon with transverse momentum [1] $p_T > 150$ GeV and $|\eta| < 2.37$, excluding the calorimeter barrel/end-cap transition regions $1.37 < |\eta| < 1.52$. The E_T^{miss} is computed as the magnitude of the

[1] ATLAS uses a cylindrical coordinate system about the beam axis with polar angle θ and azimuthal angle ϕ. Anti-clockwise beam direction defines the positive z-axis, while the positive x-axis is defined as pointing from the collision point to the centre of the LHC ring and the positive y-axis points upwards. We define transverse energy $E_T = E\sin\theta$, transverse momentum $p_T = p\sin\theta$, and pseudorapidity $\eta = -\ln(\tan(\theta/2))$.

vector sum of the transverse momentum of all noise-suppressed calorimeter topological clusters with $|\eta| < 4.9$. The energies are corrected to take into account the different response of the calorimeters to jets of hadrons, tau leptons, electrons or photons in the final state, as well as dead material and out-of-cluster energy losses [14]. The photon candidate must pass *tight* identification criteria [15] based on shower shapes measured in the electromagnetic calorimeter and on the energy leakage into the hadron calorimeter, and is required to be isolated. The energy not associated with the photon cluster in a cone of radius $\Delta R = \sqrt{(\Delta\eta)^2 + (\Delta\phi)^2} = 0.4$ around the candidate is required to be less than 5 GeV. Jets are defined using the anti-k_t jet algorithm [16] with the distance parameter set to $R = 0.4$. Measured jet p_T is corrected for detector effects, non-compensation of hadronic showers, and contributions from multiple proton-proton interactions per beam bunch crossing (pileup), as described in Ref. [17].

Events with more than one jet with $p_T > 30$ GeV and $|\eta| < 4.5$ are rejected. The reconstructed photon, $E_T^{\rm miss}$ and jets (if any) are required to be well separated in the transverse plane with $\Delta\phi(\gamma, E_T^{\rm miss}) > 0.4$, $\Delta R(\gamma, \text{jet}) > 0.4$, and $\Delta\phi(\text{jet}, \text{E}_\text{T}^{\rm miss}) > 0.4$. Additional quality criteria [18] are applied to ensure that jets and photons were not produced by noisy calorimeter cells, and to avoid problematic detector regions. Events with identified electrons or muons are vetoed to reject mainly W/Z+jets and $W/Z + \gamma$ background processes with charged leptons in the final state. Electron (muon) candidates are required to have $p_T >$ 20 GeV and $|\eta| < 2.47$ ($p_T > 10$ GeV and $|\eta| < 2.4$), and to pass the *medium* (*combined)* criteria as described in Ref. [19]. The final data sample contains 116 events, where 88 and 28 events have zero and one jet in the final state, respectively.

4 Monte Carlo simulation

The SM backgrounds to the monophoton signal are dominated by the irreducible $Z(\rightarrow \nu\bar{\nu}) + \gamma$ process, and receive contributions from $W/Z + \gamma$ events with unidentified electrons, muons or hadronic tau decays in the final state, and W/Z+jets events with an electron or jet misreconstructed as a photon. In addition, the monophoton sample receives small contributions from top quark production, $\gamma\gamma$, diboson (WW, ZZ, WZ), γ+jets, and multi-jet processes. Monte Carlo (MC) event samples are used to compute detector acceptance and reconstruction efficiencies for signal and some of the background processes, and to estimate systematic uncertainties on the final results. The W/Z+jets, γ+jets and multi-jet background contributions are determined using data, as discussed below.

Samples of simulated $W/Z + \gamma$ events are generated using ALPGEN [20] and SHERPA [21] with CTEQ6L1 [22] parton density functions (PDFs) and a photon p_T above 40 GeV. Background samples from W/Z+jets and γ+jets processes are generated for plotting kinematic distributions using ALPGEN interfaced to HERWIG [23] and JIMMY [24], also using CTEQ6L1 PDFs. Top-quark production samples are generated using MC@NLO [25] and CT10 [26] PDFs, while diboson processes are generated using HERWIG normalized to next-to-leading order (NLO) predictions with MRST2007 [27] PDFs. Finally, $\gamma\gamma$ and multi-jet processes (the latter for plotting purposes) are generated using PYTHIA [28] with MRST2007 PDFs.

Signal MC samples are generated according to the ADD LED model using the PYTHIA leading-order (LO) perturbative QCD (pQCD) implementation with default settings, minimum photon p_T of 80 GeV, and an ATLAS tune for underlying event (UE) contributions [29] that includes the use of CTEQ6L1 PDFs. The number of extra dimensions n is varied from 2 to 6 and values for M_D in the 1-2 TeV range are considered. For consistency with a previous monojet analysis performed in ATLAS [7, 8], the yields corresponding to CTEQ6.6 [30] PDFs are used, as obtained by reweighting these samples.

Simulated events corresponding to the $\chi\bar{\chi}+\gamma$ process with a minimum photon p_T of 80 GeV are generated using LO matrix elements within a MADGRAPH [31] implementation interfaced with PYTHIA for modelling the parton shower and hadronization, and using CTEQ6L1 PDFs. Values for m_χ between

1 GeV and 1.3 TeV are considered. Here WIMPs are assumed to be Dirac fermions and the vertex operator is taken to have the structure of a vector, axial-vector, or tensor, corresponding respectively to the operators D5, D8, and D9 in Ref. [12]. This corresponds to spin-independent (D5) and spin-dependent (D8 and D9) interactions.

The MC samples are generated with additional minimum bias pp interactions from PYTHIA 6 overlaid with the hard-scattering event and tuned to the data. The MC generated samples are then passed through a full simulation [32] of the ATLAS detector and trigger system, based on GEANT4 [33]. The simulated events are reconstructed and analyzed with the same analysis chain as for the data, using the same trigger and event selection criteria.

5 Background determination

The normalization of the MC predictions for the dominant $W/Z + \gamma$ background processes are set using scale factors determined in a control sample in data, resulting in a significant reduction of the background uncertainties. A $\gamma+\mu+E_T^{\rm miss}$ control sample with an identified muon in the final state is defined by inverting the muon veto in the nominal event selection criteria discussed above. According to the simulation, the sample contains a 71% contribution from $W+\gamma$ and a 19% from $Z+\gamma$ processes. This control sample is used to normalize separately the $W + \gamma$ and $Z + \gamma$ MC predictions as determined by ALPGEN and SHERPA, respectively. In each case, the scale factor is defined as the ratio between the data and the given MC prediction, after the contributions from the rest of background processes are subtracted. The latter are predicted by the MC simulation or taken from data in the case of the W/Z+jets processes. The scale factors, extracted simultaneously to take into account correlations, are: $k(W + \gamma) = 1.0 \pm 0.2$ and $k(Z + \gamma) = 1.1 \pm 0.2$, where both statistical and systematic uncertainties are included (see below).

Dedicated studies are performed to determine, using data, the probability for electrons or jets to be identified as photons in the final state, which result in data-driven estimates of W/Z+jets background contributions. A sample of Z boson candidates is employed to compute, using data, the fraction of electrons from the Z boson decay that are reconstructed as photons. This fraction decreases from 2% to 1% as p_T increases from 150 GeV to 300 GeV, and shows a moderate pseudorapidity dependence. The measured electron to photon fake rates are employed to determine the $W(\rightarrow e\nu)$+jets background in the signal region, for which a data sample selected with the nominal selection criteria and an electron instead of a photon in the final state is used. This results in a total $W(\rightarrow e\nu)$+jets background estimation of 14 ± 6 events, where the uncertainty is dominated by the limited statistics of the fake control data sample. Control samples enhanced in jets identified as photons are defined using nominal selection criteria with non-isolated photon candidates and/or photon candidates passing a *loose* selection but not the nominal identification requirements. The MC simulation indicates that the isolation is essentially uncorrelated with the details of the photon identification criteria, the latter based on the shower shape in the electromagnetic calorimeter. The ratio of isolated to non-isolated photons in the loose photon selected sample together with the number of non-isolated photons passing the nominal identification requirements are used to determine the rate of jets identified as photons in the signal region, after the contribution from $W/Z + \gamma$ processes has been subtracted. This leads to 4.3 ± 1.9 W/Z+jets background events with jets misidentified as photons in the signal region, including both statistical and systematic uncertainties associated with the method and the subtraction of the $W/Z + \gamma$ contamination.

The γ+jet and multi-jet background contributions to the signature of a photon and large $E_T^{\rm miss}$ originate from the misreconstruction of the energy of a jet in the calorimeter. The direction of $E_T^{\rm miss}$ therefore tends to be aligned with the jet. These background contributions are determined from data using a control sample with the nominal selection criteria and at least one jet with $p_T > 30$ GeV and $\Delta\phi(\text{jet}, \text{E}_\text{T}^{\text{miss}}) < 0.4$. After the subtraction of electroweak boson and top production processes, the p_T distribution of the jet is used to estimate the γ+jet and multi-jet backgrounds. A linear extrapolation of the measured p_T spec-

trum below the threshold of $p_T < 30$ GeV leads to an estimate of 1.0 ± 0.5 background events in the signal region, where the uncertainty is due to the ambiguity in the functional form used in the extrapolation. Background contributions from top quark, $\gamma\gamma$, and diboson production processes, determined using MC samples, are small. Finally, non-collision backgrounds are negligible.

6 Systematic uncertainties on background predictions

A detailed study of systematic uncertainties on the background predictions has been carried out. An uncertainty of 0.3% to 1.5% on the absolute photon energy scale [15], depending on the photon p_T and η, translates into a 0.9% uncertainty on the total background prediction. Uncertainties on the simulated photon energy resolution, photon isolation, and photon identification efficiency introduce a combined 1.1% uncertainty on the background yield. Uncertainties on the simulated lepton identification efficiencies introduce a 0.3% uncertainty on the background predictions. The uncertainty on the absolute jet energy scale [17] and jet energy resolution introduce a 0.9% and 1.2% uncertainties in the background estimation, respectively. A 10% uncertainty on the absolute energy scale for low p_T jets and unclustered energy in the calorimeter, and a 6.6% uncertainty on the subtraction of pileup contributions are taken into account. They affect the E_T^{miss} determination and translate into 0.8% and 0.3% uncertainties on the background yield, respectively. The dependence of the predicted $W/Z + \gamma$ backgrounds on the parton shower and hadronization model used in the MC simulations is studied by comparing the predictions from SHERPA and ALPGEN. This results in a conservative 6.9% uncertainty on the total background yield and constitutes the dominant source of systematic uncertainty. Uncertainties due to PDFs and the variation of the renormalization and factorization scales in the $W/Z + \gamma$ MC samples introduce an additional 1.0% uncertainty on the total background yields. Other sources of systematic uncertainty related to the trigger selection, the lepton p_T scale and resolution, the pileup description, background normalization of the top quark, $\gamma\gamma$ and diboson contributions, and a 1.8% uncertainty on the total luminosity [34] introduce a combined uncertainty of less than 0.5% on the total predicted yields. As previously mentioned, the W/Z+jets, γ+jets and multi-jet background contamination are determined from data with uncertainties between 33% and 50%. The different sources of uncertainty are added in quadrature, resulting in a total 15% uncertainty on the background prediction.

7 Results

In Table 1, the observed number of events and the SM predictions are presented. The data are in agreement with the SM background only hypothesis with a p-value of 0.2. Figure 1 shows the measured E_T^{miss} distribution compared to the background predictions. For illustration purposes the figure indicates the impact of an ADD LED and a WIMP scenario. The results are expressed in terms of model-independent 90% and 95% confidence level (CL) upper limits on the visible cross section, defined as the production cross section times acceptance times efficiency ($\sigma \times A \times \epsilon$), using the CL_s modified frequentist approach [35] and considering the systematic uncertainties on the SM backgrounds and on the integrated luminosity. Values of $\sigma \times A \times \epsilon$ above 5.6 fb and 6.8 fb are excluded at 90% CL and 95% CL, respectively.

The results are also translated into 95% CL limits on the parameters of the ADD LED model. The typical $A \times \epsilon$ of the selection criteria is 20.0 ± 0.4(stat.) ± 1.1(syst.)%, approximately independent of n and M_D. Experimental uncertainties related to the photon, jet and E_T^{miss} scales and resolutions, the photon reconstruction, the trigger efficiency, the pileup description, and the luminosity introduce a 6.8% uncertainty on the signal yield. Uncertainties related to the modelling of the initial- and final-state gluon radiation are determined using simulated samples with modified parton shower parameters and translate into a 3.5% uncertainty on the ADD LED signal yield. Systematic uncertainties due to PDFs result in a

Background source	Prediction	± (stat.)	± (syst.)
$Z(\to \nu\bar{\nu}) + \gamma$	93	± 16	± 8
$Z/\gamma^*(\to \ell^+\ell^-) + \gamma$	0.4	± 0.2	± 0.1
$W(\to \ell\nu) + \gamma$	24	± 5	± 2
W/Z + jets	18	–	± 6
top	0.07	± 0.07	± 0.01
$WW, WZ, ZZ, \gamma\gamma$	0.3	± 0.1	± 0.1
γ+jets and multi-jet	1.0	–	± 0.5
Non-collision background	–	–	–
Total background	137	± 18	± 9
Events in data (4.6 fb^{-1})	116		

Table 1: The number of events in data compared to the SM predictions, including statistical and systematic uncertainties. The quoted statistical uncertainties include both contributions from data and the limited size of the simulated samples.

0.8% to 1.4% uncertainty on the signal $A \times \epsilon$ and a 4% to 11% uncertainty on the signal cross section, increasing as n increases. Variations of the renormalization and factorization scales by factors of two and one-half introduce a 0.6% uncertainty on the signal $A \times \epsilon$ and an uncertainty on the signal cross section that varies between 11% and 22% as n increases. Figure 2 shows the expected and observed 95% CL upper limits on M_D as a function of n, as determined using the CL_s method and considering uncertainties on both signal and SM background predictions. Values for M_D below 1.74 TeV ($n = 2$ or 3), 1.78 TeV ($n = 4$), 1.82 TeV ($n = 5$), and 1.87 TeV ($n = 6$) are excluded at 95% CL. The observed limits decrease by 3% after considering the minus one-sigma uncertainty from PDFs, scale variations, and parton shower modelling in the ADD LED theoretical predictions (dashed lines in Figure 2). These results, based on LO cross sections for the signal, are conservative and improve upon previous limits on M_D.

Similarly, 90% CL upper limits on the pair production of dark matter WIMP candidates are computed. The $A \times \epsilon$ of the selection criteria are typically 18.0 ± 0.3(stat.) ± 0.9(syst.)% for the D5 and D8 operators, and 23.0 ± 0.3(stat.) ± 1.3(syst.)% for the D9 operator, with a moderate dependence on m_χ. Experimental uncertainties, as discussed above, translate into a 6.6% uncertainty on the signal yields. Theoretical uncertainties on initial- and final-state gluon radiation introduce a 3.5% to 6.0% uncertainty on the signal yields. The uncertainties related to PDFs result in 1.0% and 5.0% uncertainties on the signal $A \times \epsilon$ and cross section, respectively. Variations of the renormalization and factorization scales lead to a change of 1.0% and 8.0% in the signal $A \times \epsilon$ and cross section, respectively. Limits on the scale M_* are extracted using the CL_s method and the same prescription as for the ADD LED model. In the case of the D5 spin-independent operator, values for M_* below 585 GeV and 156 GeV are excluded at 90% CL for m_χ equal to 1 GeV and 1.3 TeV, respectively. Values for M_* below 585 GeV and 100 GeV (794 GeV and 188 GeV) are excluded for the D8 (D9) spin-dependent operator for m_χ equal to 1 GeV and 1.3 TeV, respectively. These results can be translated into upper limits on the nucleon-WIMP interaction cross section using the prescription in Ref. [12, 36]. Figure 3 shows 90% CL upper limits on the nucleon-WIMP cross section as a function of m_χ. In the case of spin-independent interactions, nucleon-WIMP cross sections above 2.2×10^{-39} cm^2 and 1.7×10^{-36} cm^2 are excluded at 90% CL for $m_\chi = 1$ GeV and $m_\chi = 1.3$ TeV, respectively. Spin-dependent interactions cross sections in the range 7.6×10^{-41} cm^2 to 3.4×10^{-37} cm^2 (2.2×10^{-41} cm^2 to 2.7×10^{-38} cm^2) are excluded at 90% CL for the D8 (D9) operator and m_χ varying between 1 GeV and 1.3 TeV. The observed limits on M_* decrease by 2% to 3% after considering the plus one-sigma theoretical uncertainty on the WIMP model. This translates into a 10% increase of the quoted nucleon-WIMP cross section limits. The exclusion in the region 1 GeV $< m_\chi <$ 3.5 GeV (1 GeV $< m_\chi <$ 100 GeV) for spin-independent (spin-dependent) nucleon-WIMP

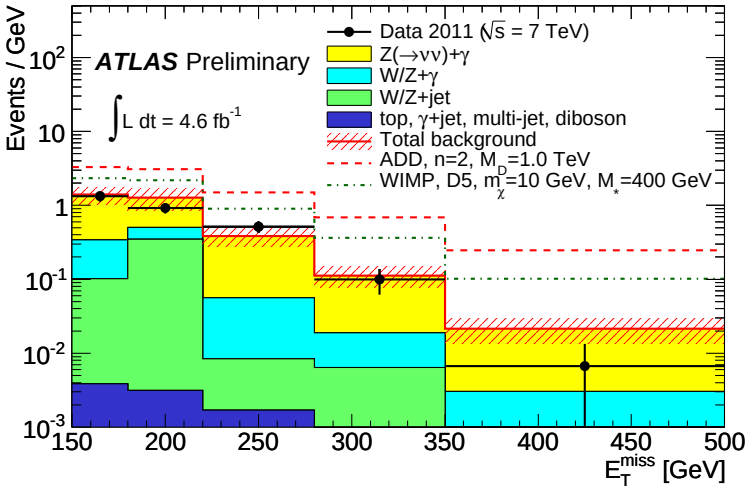

Figure 1: The measured E_T^{miss} distribution (black dots) compared to the SM (solid lines), SM+ADD LED (dashed lines), and SM+WIMP (dotted lines) predictions, for two particular ADD LED and WIMP scenarios. The background contributions from W/Z+jets, γ+jets, and multi-jet processes are taken from the MC simulations normalized to the data-driven estimations, as discussed in the text. For data only statistical uncertainties are included. The band around the total background prediction includes uncertainties on the data-driven background estimates and statistical uncertainties on the MC samples.

interactions is driven by the results from collider experiments with the assumption of the validity of the effective theory. The upper limits presented in this note improve upon CDF results at the Tevatron [4] and are similar to those obtained by the CMS experiment [6] which uses axial-vector operators to describe spin-dependent interactions.

8 Conclusion

In summary, we report results on the search for new phenomena in events with an energetic photon and large missing transverse momentum in proton-proton collisions at $\sqrt{s} = 7$ TeV, based on ATLAS data corresponding to an integrated luminosity of 4.6 fb^{-1}. The measurements are in agreement with the SM predictions for background. The results are translated into model-independent 90% and 95% confidence level upper limits on $\sigma \times A \times \epsilon$ of 5.6 fb and 6.8 fb, respectively. The results are presented in terms of new improved limits on M_D versus the number of extra spatial dimensions in the ADD LED model and upper limits on the spin-independent and spin-dependent contributions to the nucleon-WIMP elastic cross section as a function of the WIMP mass.

References

[1] OPAL Collaboration, Eur. Phys. J. C **18** 253 (2000); ALEPH Collaboration,Eur. Phys. J. C **28** 1 (2003); L3 Collaboration, Phys. Lett. B **587** 16 (2004); DELPHI Collaboration, Eur. Phys. J. C **38** 395 (2005).

[2] D0 Collaboration, Phys. Rev. Lett. **101** 011601 (2008).

[3] CDF Collaboration, Phys. Rev. Lett. **101** 181602 (2008).

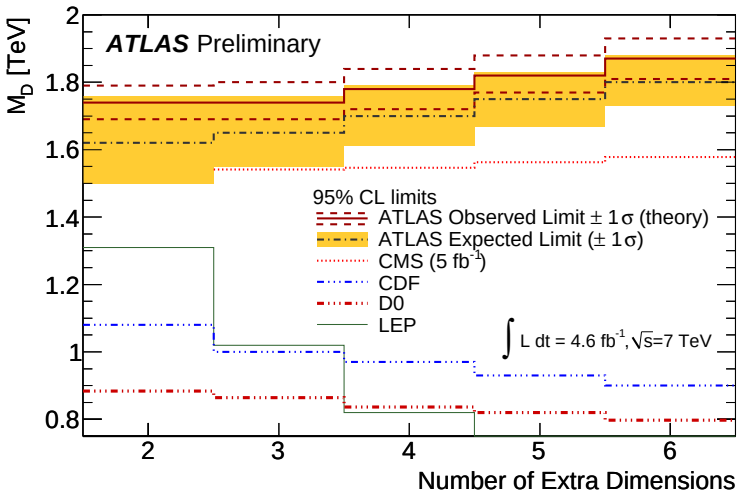

Figure 2: Observed (solid lines) and expected (dashed-dotted lines) 95% CL limits on M_D as a function of the number of extra spatial dimensions n in the ADD LED model. The dashed lines around the observed limit indicates the impact of the $\pm 1\sigma$ LO theoretical uncertainty on the limit computation. The shaded band indicates the expected $\pm 1\sigma$ range of limits in the absence of a signal. The results are compared with previous results [1, 2, 3, 6] (other lines). In the case of CMS, the result using LO signal cross sections is quoted to be comparable with this result.

[4] CDF Collaboration, Phys. Rev. Lett. **108** 211804 (2012).

[5] CMS Collaboration, Phys. Rev. Lett. **107** 201804 (2011); CMS Collaboration, arXiv:1206.5663 (2012), submitted to JHEP.

[6] CMS Collaboration, arXiv:1204.0821 (2012), submitted to Phys. Rev. Lett.

[7] ATLAS Collaboration, Phys. Lett. B **705**, 294 (2011).

[8] ATLAS Collaboration, ATLAS-CONF-2012-084 (2012).

[9] N. Arkani-Hamed, S. Dimopoulos, G.R. Dvali, Phys. Lett. B **429**, 263 (1998).

[10] WMAP Collaboration, Astrophys. J. Suppl. **192**, 18 (2011).

[11] XENON100 Collaboration, Phys. Rev. Lett. **107**, 131302 (2011); CDMS Collaboration, Phys. Rev. Lett. **106**, 131302 (2011); CoGENT Collaboration, Phys. Rev. Lett. **106**, 131301 (2011); M. Felizardo *et al.*, arXiv:1106.3014 (2011); PICASSO Collaboration, Phys. Lett. B **711**, 153 (2012).

[12] J. Goodman *et al.*, Phys. Rev D **82**, 116010 (2010), and reference therein.

[13] ATLAS Collaboration, JINST **3**, S08003 (2008).

[14] ATLAS Collaboration, Eur. Phys. J. C **72**, 1844 (2012).

[15] ATLAS Collaboration, Phys. Rev. D **85**, 092014 (2012).

[16] M. Cacciari, G. P. Salam and G. Soyez, JHEP **0804**, 063 (2008).

[17] ATLAS Collaboration, arXiv:1112.6426, submitted to Eur. Phys. J. C.

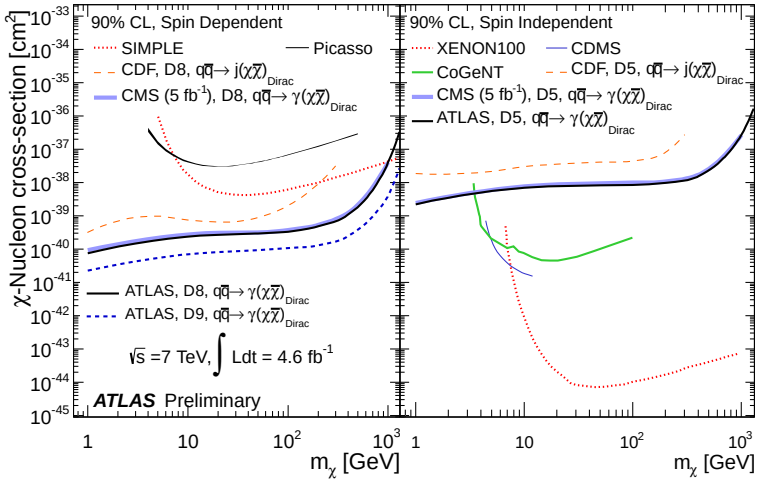

Figure 3: 90% CL upper limits on the nucleon-WIMP cross section as a function of m_χ for spin-dependent (left) and spin-independent (right) interactions, corresponding to D8, D9, and D5 operators in Ref. [12, 36]. The results are compared with previous CDF [4] and CMS [6] results and results from direct WIMP detection experiments [11]. The CMS limit curve generally overlaps the ATLAS curve.

[18] ATLAS Collaboration, ATLAS-CONF-2012-020 (2012).

[19] ATLAS Collaboration, Phys. Rev. D **85**, 072004 (2012).

[20] M.L. Mangano *et al.*, JHEP **0307**, 001 (2003).

[21] T. Gleisberg, S. Hoeche, F. Krauss, M. Schoenherr, S. Schumann, F. Siegert, J. Winter, JHEP **0902**, 007 (2009).

[22] J. Pumplin *et al.*, JHEP **0207**, 012 (2002).

[23] G. Corcella *et al.*, JHEP **0101**, 010 (2001).

[24] J. Butterworth, J. Forshaw and M. Seymour, Z. Phys. C **72**, 637 (1996).

[25] S. Frixione, B.R. Webber, Cavendish-HEP-08/14, arXiv:hep-ph/0812.0770.

[26] H-L. Lai *et al.*, Phys. Rev. D **82**, 074024 (2010).

[27] A. D. Martin, W. J. Stirling, R. S. Thorne, and G. Watt, Eur. Phys. J. C **63** 189 (2009).

[28] T. Sjöstrand *et al.*, JHEP **0605**, 026 (2006).

[29] ATLAS Collaboration, ATL-PHYS-PUB-2010-014 (2010).

[30] P. M. Nadolsky *et al.*, Phys. Rev. D **78**, 013004 (2008).

[31] J. Alwall *et al.*, JHEP **6**, 128 (2011).

[32] ATLAS Collaboration, Eur. Phys. J. C **70**, 823 (2010).

[33] S. Agostinelli *et al.*, Nucl. Instrum. and Methods A **506**, 250 (2003).

[34] ATLAS Collaboration, ATLAS-CONF-2012-080 (2012).

[35] T. Junk, Nucl. Instrum. Meth. A **434**, 435 (1999).

[36] In consultation with the authors of [12], a factor $4.7 \times 10^{-39}\text{cm}^2$ is used in the cross section formula for D8 and D9 operators instead of the quoted $9.18 \times 10^{-40}\text{cm}^2$ to fix a typographical mistake.